Supplement of Atmos. Chem. Phys., 16, 5283–5298, 2016
http://www.atmos-chem-phys.net/16/5283/2016/
doi:10.5194/acp-16-5283-2016-supplement

Atmospheric Chemistry and Physics Open Access EGU

Supplement of

NO_x lifetimes and emissions of cities and power plants in polluted background estimated by satellite observations

Fei Liu et al.

Correspondence to: S. Beirle (steffen.beirle@mpic.de) and Q. Zhang (qiangzhang@tsinghua.edu.cn)

1. Impact of interfering sources on a simple lifetime fit

In recent studies, the decay of NO_2 downwind from strong NO_x emission sources was used to derive the NO_x lifetime. However, this method can be strongly affected by neighboring sources. In a case study, we investigated the effect of an interfering source 100 km downwind with 10% of the emission rate as the source of interest. If such an interference is not accounted for by the fitted model function (e.g. in Beirle et al., 2011), the fit tries to "explain" the downwind interference by a higher lifetime. In the example shown in Fig. S1, a 10% of interference results in a 20% longer lifetime.

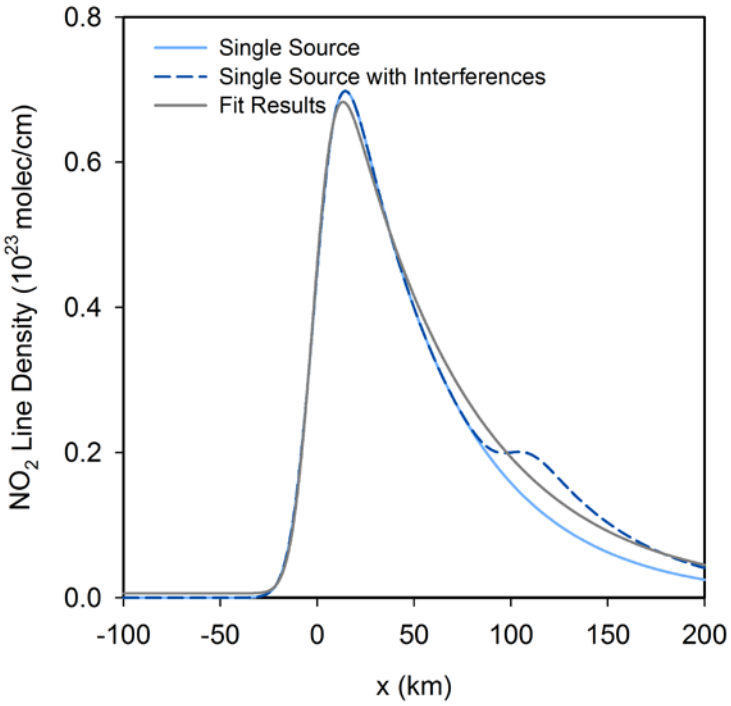

Figure S1. Sensitivity of the fitted lifetime to interferences. Solid blue line: synthetic line densities of a single source with emissions of 500 molec-NO_2/s, assuming a pseudo first-order loss of NO_2 for a a-priori lifetime of 3 hours and a wind speed of 5 m/s with a spatial smoothing following a Gaussian function with a standard deviation of 10 km; blue dash: line densities of the single source with an additional source with emissions of 50 molec-NO_2/s at 100 km. Grey: lifetime fit based on *M(x)* (Eq. 1).

2. Investigated Locations

In this study, 24 power plants and 69 cities across China and the US are investigated, including 7 power plants and 16 cities located in mountainous regions, as listed in Table S2.

Table S2 Summary of power plants and cities investigated in this study.

Category	ID	Location	Latitude	Longitude	Lifetime			Emission (mol/s)	
					Value	Num[a]	SD[a]	This Study	Bottom-up
Power Plants	1	Shangdu	42.2	116.0	2.3	3	0.6	20	17
	2	Shimen	29.6	111.4	3.6	1	-	7	8
	3	Tuoketuo	40.2	111.4	3.7	6	2.9	56	57
	4	Xinyang	32.1	114.1	3.3	5	1.2	8	11
	5	Xuzhou	34.4	117.3	5.4	3	4.0	63	58
	6	Yangcheng	35.5	112.6	7.5	3	4.1	30	24
	7	Colstrip	45.9	-106.6	3.7	4	1.3	11	14
	8	Conemaugh	40.5	-79.1	3.7	3	0.2	13	19
	9	Coronado	34.5	-109.3	2.0	3	0.4	9	9
	10	Crystal River	29.0	-82.7	3.1	6	1.2	13	16
	11	George Neal North	42.3	-96.4	2.5	5	0.8	15	11
	12	Harllee Branch	33.2	-83.3	4.4	5	1.6	12	12
	13	Hunter	39.3	-111.1	2.1	4	0.6	29	19
	14	Joppa Steam	37.2	-88.9	3.4	7	1.4	12	15
	15	Laramie River	42.1	-104.9	1.9	3	0.3	16	11
	16	Powerton	40.6	-89.6	3.9	6	1.1	11	13
	17	Rockport	37.9	-87.0	3.3	5	0.7	19	16
Cities	18	Pingdingshan	33.7	113.2	4.2	3	1.6	69	46
	19	Changchun	43.9	125.4	3.8	5	0.8	37	94

	20	Changsha	27.9	113.0	3.5	4	0.7	39	51
	21	Changzhi	36.3	113.2	3.4	2	0.9	65	42
	22	Chongqing	29.5	106.3	3.2	1	-	88	44
	23	Dalian	39.0	121.8	5.1	4	1.2	41	60
	24	Daqing	46.6	125.1	3.8	5	0.8	26	88
	25	Hangzhou	30.2	120.4	4.3	4	1.5	60	69
	26	Harbin	45.8	126.7	3.5	5	0.6	58	72
	27	Huainan	32.7	117.0	5.2	5	1.8	41	52
	28	Jinan	36.9	117.9	6.4	1	-	181	79
	29	Jiujiang	29.8	116.0	2.7	3	0.0	33	27
	30	Kunming	25.0	102.8	3.9	2	0.9	23	50
	31	Linyi	35.1	118.3	5.3	5	2.3	16	40
	32	Liuzhou	24.3	109.4	2.8	2	0.9	26	31
	33	Nanning	22.8	108.4	3.7	3	2.8	10	20
	34	PRD	22.8	113.5	3.7	3	0.4	433	493
	35	Qingdao	36.1	120.2	4.2	2	4.3	70	76
	36	Qiqihar	47.2	123.6	4.3	4	1.4	20	27
	37	Shanghai	31.3	121.5	4.7	4	1.4	322	271
	38	Tangshan	39.7	118.2	3.9	3	0.6	162	141
	39	Tianjin	39.1	117.3	3.7	4	0.5	145	100
	40	Tonghua	41.8	126.0	3.6	3	1.2	16	15
	41	Wuhan	30.6	114.3	2.6	4	0.8	185	130
	42	Xiamen	24.5	118.1	3.4	1	-	89	72
	43	Xiangyang	32.0	112.1	2.9	1	-	41	39
	44	Yinchuan	38.5	106.2	3.5	5	0.9	33	28
	45	Yueyang	29.4	113.1	2.6	5	2.1	28	24
	46	Zhanjiang	21.3	110.3	3.7	3	0.7	11	22

	47	Atlanta	33.8	-84.4	5.1	4	3.7	29	35
	48	Chicago	41.8	-87.7	3.9	8	1.4	209	92
	49	Cincinnati	39.1	-84.6	4.2	5	1.3	43	22
	50	Cleveland	41.5	-81.7	4.6	6	3.4	11	33
	51	Columbus	40.0	-83.1	5.6	4	1.5	7	22
	52	Dallas	32.9	-97.0	3.9	4	0.7	77	39
	53	Detroit	42.4	-83.1	4.5	6	2.6	100	61
	54	Houston	29.8	-95.3	3.5	4	0.9	78	50
	55	Indianapolis	39.8	-86.2	4.7	3	2.4	17	21
	56	Jacksonville	30.5	-81.6	3.2	5	1.1	23	30
	57	Kansas City	39.2	-94.6	3.5	2	0.1	32	27
	58	Memphis	35.1	-90.1	3.0	3	0.7	11	21
	59	Miami	26.0	-80.2	4.7	2	0.1	39	36
	60	Minneapolis	45.0	-93.3	3.8	5	0.7	62	44
	61	Montreal	45.6	-73.7	2.5	4	0.9	59	59
	62	New Orleans	30.1	-90.3	4.9	6	2.3	15	14
	63	New York	40.7	-73.5	4.4	5	0.9	247	311
	64	Omaha	41.3	-96.1	2.0	5	1.4	32	25
	65	Orlando	28.5	-81.3	3.5	5	1.0	24	25
	66	Philadelphia	40.0	-75.2	4.4	5	1.2	55	65
	67	San Antonio	29.6	-98.5	3.4	3	0.5	20	16
	68	St Louis	38.7	-90.4	3.7	5	1.2	56	36
	69	Tampa	27.9	-82.4	3.7	6	1.6	39	28
	70	Tucson	32.3	-110.9	1.8	3	0.5	21	11
Mountainous Power Plants	71	Daba	38.0	105.9	3.5	4	1.2	86	24
	72	Jingyuan	36.7	104.8	1.6	2	0.8	14	19
	73	Shentou	39.4	112.6	2.9	3	0.2	73	52

	74	Cholla	34.9	-110.3	1.9	1	-	21	8
	75	Four Corners	36.8	-108.4	2.2	2	0.5	83	44
	76	Intermountain	39.5	-112.6	2.1	5	0.8	39	19
	77	Navajo	36.9	-111.4	3.1	3	0.8	18	22
Mountainous Cities	78	Baotou	40.6	109.8	4.3	7	3.4	94	82
	79	Beijing	39.8	116.3	2.5	4	0.9	252	109
	80	Chifeng	42.3	119.3	2.5	5	0.9	26	25
	81	Datong	40.1	113.3	3.3	3	0.4	106	70
	82	Hohhot	40.8	111.7	4.1	6	3.1	26	38
	83	Lanzhou	36.1	103.8	2.0	1	-	35	47
	84	Shijiazhuang	38.1	114.5	4.0	2	0.6	261	72
	85	Taiyuan	37.6	112.4	2.9	2	1.5	180	78
	86	Wenzhou	28.0	120.7	7.9	1	-	18	46
	87	Zhangjiakou	40.8	114.8	2.4	3	0.7	64	43
	88	Denver	39.8	-105.0	2.6	1	-	78	47
	89	Las Vegas	36.2	-115.2	1.7	3	0.1	68	31
	90	Phoenix	33.6	-112.0	1.3	2	1.0	138	36
	91	Portland	45.5	-122.6	2.8	1	-	73	33
	92	Salt Lake City	40.7	-112.0	1.9	3	1.1	87	20
	93	Seattle	47.4	-122.3	1.4	1	-	232	29

[a]Num: the number of fits for wind direction sectors with a good fit performance; SD: the standard deviation of fits for wind direction sectors with a good fit performance.

3. Uncertainties

We here investigate the different sources of uncertainties contributing to the overall uncertainties of the derived lifetimes and emissions. For both τ and emissions, the choice of integration and fit intervals (a), confidence intervals and variability of fit results (b), and wind fields (c) contribute to the uncertainties. In addition, uncertainties in the total NO_2 mass fit (d), tropospheric NO_2 TVCDs (e) and the NO_2/NO_x ratio (f) affect the derived emissions. In (g), we discuss potential errors due to the assumption of having a single effective lifetime.

(a) Choice of integration and fit intervals

Analogue to Beirle et al. (2011), we investigate the impact of the a-priori choice of integration and fit intervals. The fitted τ is generally robust with respect to changes of the fit interval *f* and integration interval *i* for the calculation of *C(x)* in *N(x)*, associated with the good representation of the emission pattern provided by the NO_2 distribution under calm wind condition *C(x)* in any case. A change of *f* and *i* by ± 100 km affects the resulting lifetimes by only about 10%. The dependency of the fit results for τ and emissions on the fit and integration intervals and choice of wind fields are tabulated in Table S1.

(b) Fit errors

The fit errors expressed as 95% confidence interval (CI) are derived from the least-squares fit routine directly for individual sources. They are typically of the order of 30% for τ and 20% for *A*, respectively. In addition, for τ, the standard mean error of fitted lifetimes for all wind direction sectors is regarded as a measure of uncertainty to reflect the reliability of lifetimes. But for 5 sites, the fit of τ can only work for a single direction and not allow for statistical analysis. We thus average the standard deviation of τ for all available sites, yielding 40%, and calculate the lifetime uncertainty as standard mean error (i.e., 40%/sqrt(n), with n being the number of available wind directions., i.e. 20% if 4 wind directions are available).

(c) Wind fields

The accuracy of wind fields affects our analysis twofold, by sorting the NO_2 TVCDs according to wind directions as well as by transferring the fitted e-folding distance into a lifetime. We choose ECMWF wind fields averaged from ground up to 500 m and a threshold of 2 m/s for calm winds in this study. Uncertainties due to the choice of layer height (e.g. 200 m or 1000 m) are comparable with Beirle et al. (2011): the resulting lifetimes/emissions

change about 10% on average. We also investigate the dependency on the choice of the threshold for calm wind. The threshold of 2 m/s was found to be a good compromise of sufficient sample size for both the calculation of line densities for calm as well as for windy conditions. It successfully worked out for 70 non-mountainous sites, while for both lower and higher thresholds (of e.g. 1 m/s and 3 m/s), several sites are discarded, due to low sample sizes for calm (implying a bad representation of the emission pattern) and noisy downwind patterns, respectively. Thus we consider that the threshold of 2 m/s is optimal in this study.

In addition, we carried out a comparison of wind information between ECMWF and sounding measurements (Table S3). Here we focus on the comparison of the quantity used for the lifetime estimate, i.e. the projected wind components for each wind direction sector. We firstly sorted ECMWF wind fields for the years 2005–2013 into 8 wind direction sectors and classified the simultaneous sonde data into the same wind direction sector, and then calculate the mean of the projected wind speeds from both datasets to compare. While *total* wind speeds from ECMWF and sonde measurements agree quite well (~5% on average for wind speeds>2 m/s), the *projected* wind components are systematically higher for ECMWF. This can be expected, as ECMWF wind fields are the basis for the wind direction classification. If, for instance, the true wind would be 5 m s^{-1} from north, but the model wind is 5 m s^{-1} from east, the case is classified as easterly, while the actual easterly wind component is 0. That is, deviations of the wind direction (even if 0 on average) cause a systematic bias due to this projection procedure. Thus, the deviation of the projected wind speeds reflects uncertainties of the sorting procedure caused by deviations of the wind direction, and allows for an estimate of the overall uncertainty due to wind fields. The deviations for non-mountainous sites are, on average, acceptable (26%). Note also that de Foy et al. (2015) report on ERA-Interim winds yielding a better lifetime estimate compared to the North American Regional Reanalysis project (NARR). For mountainous sites, however, significantly higher deviations are found (37% on average) due to insufficient spatial resolution of ECMWF (see also Sect. 2.6 of the manuscript).

Wind fields often reveal systematic spatio-temporal patterns, such as diurnal cycles or land-sea transitions, which could have systematic effects on our results. As the underlying physical processes are included in the models, these effects should, in first order, be accounted for by ECMWF. However, the spatial resolution might be too coarse to capture these effects completely.

Beirle et al. (2011) varied the time of the wind data used for the fit and found changes below 10%. In addition, from the comparison with sonde data, we see no indication that ECMWF data are particularly biased for coastal cities (Miami, Xiamen). We thus consider the uncertainties caused by diurnal cycles of wind speeds or land-sea transitions to be covered by the estimated overall uncertainty related to wind fields.

Overall, we estimate the uncertainties associated with the wind data as 30% for non-mountainous sites.

(d) Fit of the total NO_2 mass

The emission estimate is based on the spatially integrated NO2 VCD above background (Eq. (5)). The integration interval aligned in the wind direction *h* and fit interval aligned in the across-wind direction *v* (see Fig. S2) was chosen in order to allow a robust fit of the total NO_2 mass on top of the background. If *h* and *v* are chosen too small, emissions are underestimated caused by the loss of part of the NO_2 TVCDs from the source of interest; while, if *h* and *v* are chosen too large, interferences from surroundings are included and the derived emissions are not from the target source, but from a larger area (compare the next section). The fitted emissions are rather insensitive to the change of *v*, because possible losses by cross-wind dilution are accounted for by scaling the integrated NO_2 mass according to the fitted width of the Gaussian plume. The resulting emissions change about 5% on average when *v* is increased by 50%. If the fit interval *h* is increased by 50% as well, the emissions for fewer sites (66 sites) can be estimated, related to the enhanced interferences corresponding to larger *h* which cannot be simply interpreted by linear background (i.e., $\varepsilon_i+\beta_i x$ in Eq. (5)), thus justifying the choice of *h* as reasonable. The fitted emissions are also found to be not very sensitive to the choice of *h: A* increases by only ~20% when *h* increases by 150%. We estimate the uncertainties due to the fit of the total NO_2 mass as 20%, and apply this number to all considered sources.

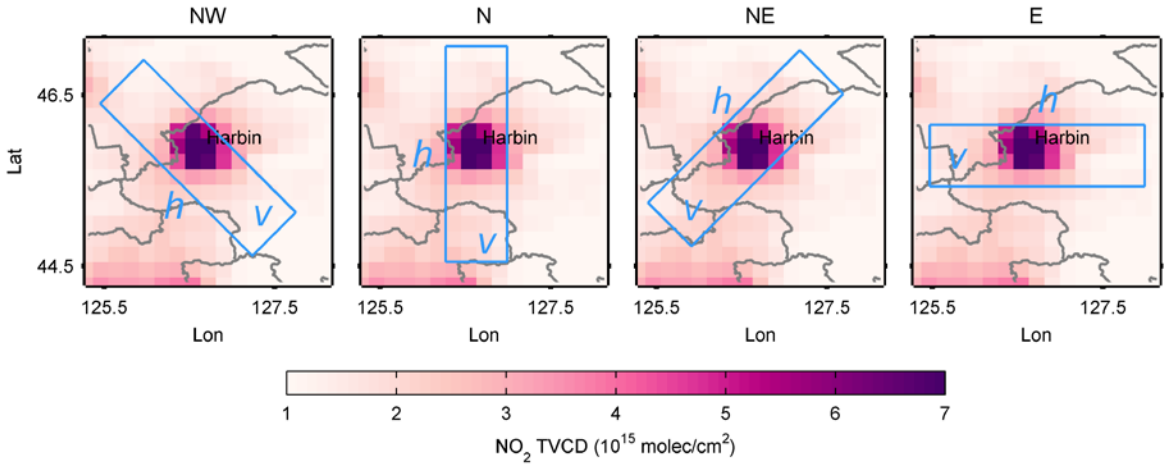

Figure S2. The intervals chosen for the fit of total NO_2 mass for northwest, north, northeast and east directions (from left to right). The mean calm NO_2 TVCDs are integrated over interval *v* to calculate line densities and the fit is performed over the interval *h* (see Sect. 2.2.3).

(e) Tropospheric NO_2 TVCDs

The uncertainty of TVCDs consists of additive (biases due to the spectral retrieval and the stratospheric correction) and multiplicative terms (tropospheric AMFs). For our study, any additive bias is eliminated by the fitted background, while the uncertainty of the tropospheric AMF of about 30% (Boersma et al., 2007, table 2 therein) directly propagates to the uncertainty of the estimated emissions. Note that this is a quite conservative estimate, as all statistical error components are strongly suppressed in this analysis due to the consideration of multiannual means.

The retrievals of NO_2 TVCDs performed by KNMI (used in this study) and NASA (OMI "Standard Product") are based on the same spectral analysis, but differ in the separation of stratospheric and tropospheric columns and AMF calculations (Bucsela et al., 2013; Boersma et al., 2011; Boersma et al., 2007; Dirksen et al., 2011), which resulted in some significant differences in their early released products (Lamsal et al., 2010; Platt and Stutz, 2008). With the development of NO_2 retrieval algorithms, however, the two products are increasingly converging (Bucsela et al., 2013; Boersma et al., 2011).

Though the recent update of the DOMINO algorithm (Boersma et al., 2011) has improved some issues related to the spatial resolution of external databases, retrievals are still based on relatively coarsely resolved terrain height, ground albedo, and a-priori NO_2 vertical profile shape, probably causing low-biased VCDs over strong emission sources (e.g., Russell et al., 2011). These effects are, however, covered by the assumed uncertainty of TVCDs of 30%.

Recently, an overall bias of the OMI NO_2 column density has been reported, which turns out to be related to an imperfect spectral analysis and could be removed by improved spectral fitting procedures (van Geffen et al., 2015; Marchenkov et al., 2015). Unfortunately, the updated datasets are not available yet.

However, as an overall bias in total columns is mostly removed by the stratospheric correction procedures, we do not expect a large effect on the tropospheric NO_2 column densities over polluted sites, and thus no impact on our emission estimates.

In this study, only cloud-free NO_2 TVCDs are used for fitting lifetimes and emissions, which do not represent the average level for all days due to the accelerated photochemistry and different meteorological conditions (e.g. boundary layer height, atmospheric transport) under clear sky conditions. But still the emission estimates are appropriate, as both the NO_x lifetime and total mass derived from the NO_2 TVCDs are derived consistently, both of which reflect the values under clear sky conditions. Thus, this effect is of minor importance for this study and is not expected to bias the estimates of NO_x emissions.

(f) The NO_x/NO_2 ratio

The derived emissions in terms of NO_2 are upscale to NO_x based on a constant NO_x/NO_2 ratio of 1.3, representing "typical urban conditions and noontime sun" (Sect. 6.5.1 of Seinfeld and Pandis, 2006). Note that conditions are quite consistent in this study due to the overpass time of OMI close to noon, the selection of cloud-free observations, the focus on the ozone season, and the focus on polluted regions with generally high tropospheric ozone. In addition, we have checked the NO_x/NO_2 ratio at OMI overpass time within the boundary layer (up to 2 km) with the CTM EMAC (Jöckel et al., 2015) and found values of 1.28 $\pm$ 0.08 for polluted ($NO_x > 1 \times 10^{15}$ molec/cm^2) regions in China and the US for the 1st of July 2005, and similar values for all days of the ozone season (on average 1.32 $\pm$ 0.06).

However, the NO/NO_2 ratio of course might differ locally, in particular when the difference in O_3 concentrations between upwind and downwind plumes is significant. But the influence is not dramatic on the scales of the OMI footprint (at least 13 km $\times$ 24 km). In addition, the influence has been included in the overall uncertainty estimates by averaging the fit results for different wind direction sectors that usually represent different levels of incoming O_3. We consider the applied correction (with an assumed uncertainty of 10%), to be adequately represented by the CTM, reflecting the mean conditions over spatial scales of ~100−200 km.

(g) General approach

In this study, we assumed that the removal of NO_2 can be simply described by a first order loss, and thus the chemical decay of NO_2 follows an exponential decay function $e(x)$ (Eq. 2) with an e-folding distance x_0, which yields an overall, effective lifetime τ. From the very good lifetime fit performance, we see no indications that this assumption is insufficient. In Beirle et al. (2014), it was investigated how far the estimated lifetime by a similar approach might be biased in case of temporal fluctuations of both emissions and instantaneous lifetimes. The impact of such fluctuations was found to be rather small.

In Eq. (4), it is implicitly assumed that the lifetime is the same for calm and windy conditions. We thus checked the mean NO_2 TVCDs for calm and windy conditions and find small (<10%), but systematic differences (Fig. S5), which are likely related to changes in lifetimes under different wind conditions. Valin et al. (2013) argue that higher wind speeds cause faster dilution of NO_x, leading to longer lifetimes. This effect could contribute to the observed larger NO_2 TVCDs under windy conditions compared to calm wind conditions. However, it is interesting to note that for some sites, NO_2 TVCDs are also larger under calm wind conditions. A better understanding of the dependence of NO_2 column densities on wind conditions thus probably requires the consideration of various parameters influencing the NO_x chemistry. The effect is rather small (less than 10% on average, see Fig. S5), we thus estimate the uncertainties due to the potential dependence of lifetimes (and other factors) on wind conditions as 10%.

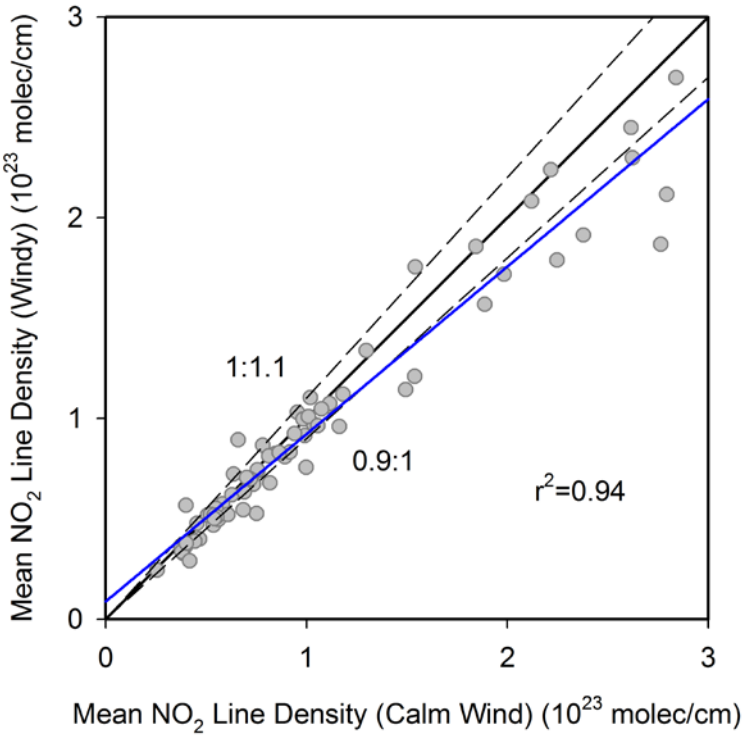

Figure S5. Scatterplot of mean NO_2 line densities under calm wind condition versus under windy condition. NO_2 line densities (integration interval: 300 km) for non-mountainous power plants and cities are averaged over the fit interval (600 km). Only those wind directions are included for which the fit works properly. The blue line represents the fitted regression line with a slope of 0.8 and an intercept of 0.1. The ratio of mean NO_2 line density under windy wind condition to that under calm wind condition is 0.9.

Table S1. The mean relative change of resulting lifetime τ and emission E for different choices of fit and integration intervals, and wind fields.

	f+100	f−100	i+100	i−100	h×150%	v×150%	⩽1 m/s[a]	⩽3 m/s[a]	200m[b]	1000m[b]
mean[$(\Delta\tau)/\tau$]	-2%	-4%	7%	8%	—	—	-5%	2%	7%	-8%
mean[$(\Delta\tau)$]/mean[τ]	-4%	-4%	6%	5%	—	—	-9%	2%	7%	-9%
mean[$(\Delta\tau)$]	-0.2	-0.2	0.2	0.2	—	—	-0.3	0.1	0.3	-0.4
mean[(ΔE)/E]	7%	8%	-2%	2%	14%	1%	7%	0%	-5%	13%
mean[(ΔE)]/mean[E]	5%	5%	-3%	12%	22%	6%	0%	-1%	-3%	11%
mean[(ΔE)]	3.4	3.3	-2.2	7.3	13.2	0.6	-0.2	-0.5	-2.0	6.0
N[c]	69	70	69	69	66	69	19	64	67	69

[a]definition of calm wind

[b]the height that ECMWF wind fields averaged from ground up to

[c]the number of sources for which the modified method in this study can work out

Table S3. Comparison of average wind speeds for years 2005−2013 for available cities from ECMWF and sounding measurements assembled by University of Wyoming.

City	Projected Speed (m/s)[a]		Percent Difference[b]	r^2	Unprojected Speed (m/s)[a]		Percent Difference[b]	Elevation Difference (m)[c]
	ECMWF	Sounding			ECMWF	Sounding		
Miami	4.8	4.0	+15%	0.59	4.9	4.5	+7%	0
Harbin	7.0	5.6	+20%	0.67	7.1	6.3	+11%	-6
Wuhan	4.6	3.2	+31%	0.63	4.7	4.5	+3%	25
Omaha	7.8	6.4	+18%	0.77	8.0	7.0	+12%	33
Kunming	7.0	5.0	+28%	0.72	7.1	6.1	+15%	36
Changsha	4.9	2.8	+43%	0.61	4.9	4.4	+12%	73
Xiamen	6.2	5.0	+19%	0.65	6.3	5.7	+8%	77
Chongqing	3.9	2.2	+43%	0.30	4.0	3.7	+7%	85
Non-mountainous cites	5.8	4.3	+26%	0.62	5.9	5.3	+10%	40
Chifeng	5.8	3.3	+43%	0.42	5.9	4.7	+21%	273
Phoenix	3.6	3.0	+18%	0.19	3.7	4.6	-25%	315
Beijing	4.5	3.9	+14%	0.56	4.6	5.1	-10%	319
Lanzhou	4.7	2.4	+48%	0.41	4.7	3.9	+16%	416
Salt Lake City	4.0	2.8	+29%	0.30	4.0	4.5	-13%	479
Taiyuan	4.9	2.5	+49%	0.42	4.7	4.3	+9%	410
Denver	3.5	1.8	+50%	0.12	3.6	3.9	-9%	637
Mountainous cites	4.4	2.8	+37%	0.35	4.5	4.4	+1%	429

[a]Average of wind speeds (>2 m/s) for each wind direction sector (see Sect.2.6 for detail)

[b]Percent Difference = (speed in ECWMF - speed in sounding) / speed in ECWMF

[c]Elevation Difference = elevation in ECWMF - elevation in GTOPO

4. Impact of distances between sources on fitted emissions

As for the distance between sources, we find that it is not critical for the fit of lifetime, as the actual distribution of sources is appropriately accounted for by *C(x)*. But for the fit of the total mass, a decision of the extent of the source under investigation has to be made. Here, we define the extent of the city to be $\pm$20 km and integrate the calm VCDs in across-wind direction over this interval. Thus, any interference within 20 km will automatically be assigned to the source of interest.

We performed a sensitivity analysis to investigate the effect of the distance between sources on the estimate of emissions. We simulated the line densities of a single source with emissions of 500 molec-NO_2/s and with an additional source with emissions of 10%, 25% and 100% of the source of interest at 0–50 km distance, respectively, assuming an a-priori lifetime of 3 hours with a spatial smoothing following a Gaussian function with a standard deviation of 10 km. We then performed a non-linear least-squares fit of the modified Gaussian function *g(x)* (Eq. (5)) to the synthetic line densities, as illustrated in Fig. S7.

Generally, the fit cannot distinguish the source and the interference within 20 km, which tries to "explain" the interference by a larger emission. In the examples shown in Fig.S7, a 10%–100% of interference results in emission estimates which generally include the interfering source. From a distance of 30 km on, the performance of the fit gets more and more unstable, due to the interference. For distances of 40 km (and larger), the fit works properly again with a bias of less than 5% for most cases, and correctly separates the source of interest from the interfering source.

However, if the interference is comparably large as the source (500 molec-NO_2), uncertainties are large. Thus, we conclude that our method generally is applicable for regional dominant sources within about a radius of 100 km. Interfering sources within 20 km cannot be separated, but will be included in the emission estimate. From 40 km on, interfering sources will not be included.

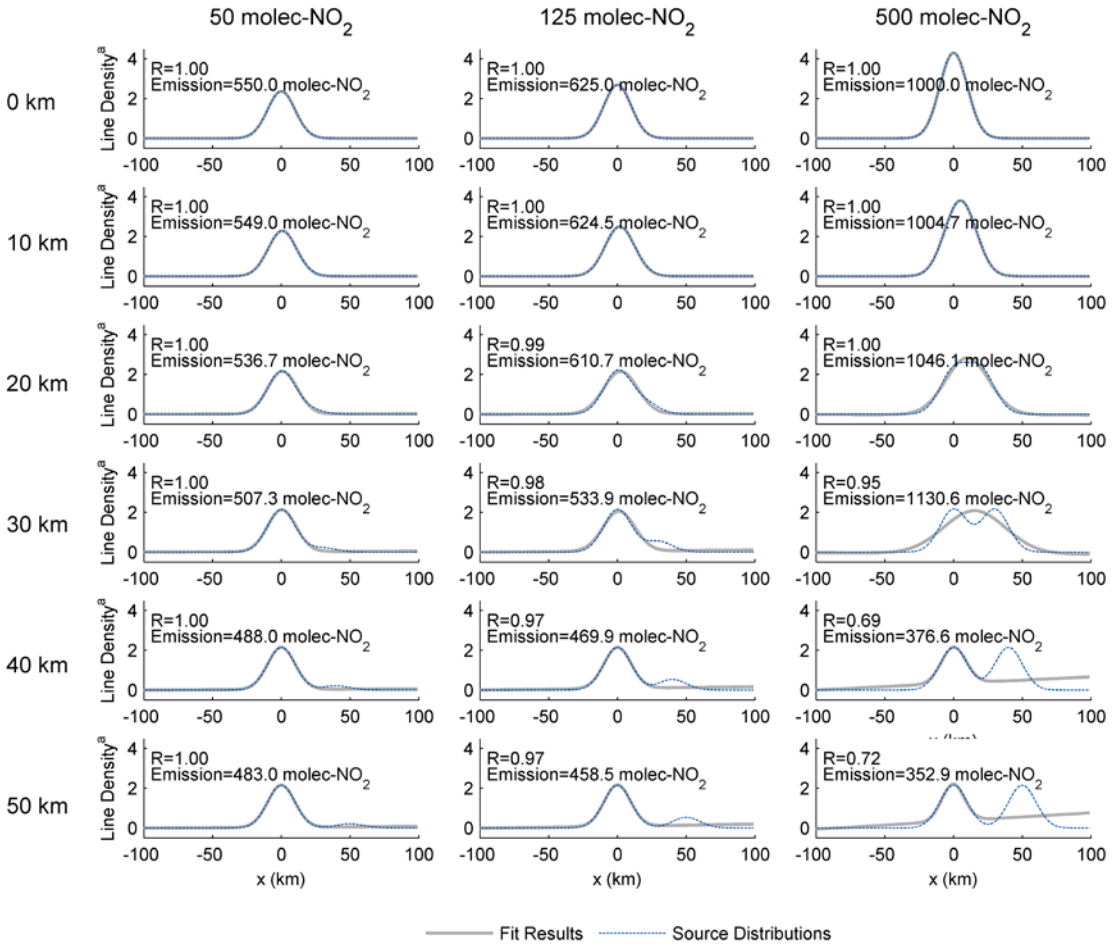

Figure S7. Sensitivity of the fitted emission to the distance between sources. Blue dot: synthetic line densities of a single source with emissions of 500 molec-NO_2/s under calm wind condition and with an additional source with emissions of 50, 125 and 500 molec-NO_2/s (from left to right) at 0–50 km (from top to bottom). Grey: emission fit based on *g(x)* (Eq. 5). The number indicates Emission resulting from the least-squares fit with 95% CI.

[a]Line Density: NO_2 line density (10^{23} molec/cm)

5. Potential applications for SO_2

We have presented a method for the estimation of NO_x lifetimes and emissions from space for strong sources on top of a generally polluted background.

Satellite observations of SO_2 have been used before for top-down estimates of emissions (e.g., Fioletov et al. (2011)) and even to obtain estimates of SO_2 lifetimes under special circumstances. Beirle et al. (2014) analyzed downwind plume evolution of SO_2 from the Kilauea volcano on Hawaii and estimated the respective SO_2 lifetime and emissions by a method similar to that proposed in Beirle et al. (2011) for NO_2. In this special case, however, wind conditions were pretty stable, and only one main wind direction had to be considered, without any sorting, due to the prevailing trade winds.

For multiple sources in polluted background and variable wind conditions, however, the situation for SO_2 is much more complex than for NO_2: The NO_2 observations are sorted according to the wind direction at the time of the measurement, while the "history" (i.e. the potential impact of NO_x emissions from the previous day, transported under possibly different wind conditions) is not considered. While this is appropriate for NO_2 due to the lifetime of a few hours, this is fundamentally different for SO_2 with longer lifetimes, which causes considerably higher uncertainties due to changes of wind directions. In addition, also the across-wind integration (needed to compensate for spatial dilution) as well as the fit would have to be performed on larger intervals for longer lifetimes, such that nearby sources cannot be separated from each other anymore and the quantification of SO_2 emissions from an individual source would be more difficult.

Thus, it might be worth testing a similar method for SO_2, but one has to be aware of the potential drawbacks, and we expect a higher uncertainty of resulting emissions as a consequence of the generally longer lifetime of SO_2.

Other Tables and Figures

Table S4. Topographic information of power plants and cities defined as mountainous sites.

ID	Location	Lifetime	Elevation in GTOPO (m)	Elevation in ECMWF (m)	Elevation Difference (m)
71	Daba	3.5	1121	1373	252
72	Jingyuan	1.6	1491	1824	333
73	Shentou	2.9	1057	1405	348
74	Cholla	1.9	1548	1838	290
75	Four Corners	2.2	1628	1918	290
76	Intermountain	2.1	1420	1671	250
77	Navajo	3.1	1358	1720	362
78	Baotou	4.3	1043	1331	288
79	Beijing	2.5	40	359	319
80	Chifeng	2.5	481	754	273
81	Datong	3.3	1027	1350	323
82	Hohhot	4.1	1046	1412	366
83	Lanzhou	2.0	1743	2159	416
84	Shijiazhuang	4.0	76	341	265
85	Taiyuan	2.9	799	1208	410
86	Wenzhou	7.9	18	329	311
87	Zhangjiakou	2.4	738	1203	465
88	Denver	2.6	1610	2247	637
89	Las Vegas	1.7	638	1031	393
90	Phoenix	1.3	339	654	315
91	Portland	2.8	67	364	297
92	Salt Lake City	1.9	1297	1776	479
93	Seattle	1.4	36	369	333

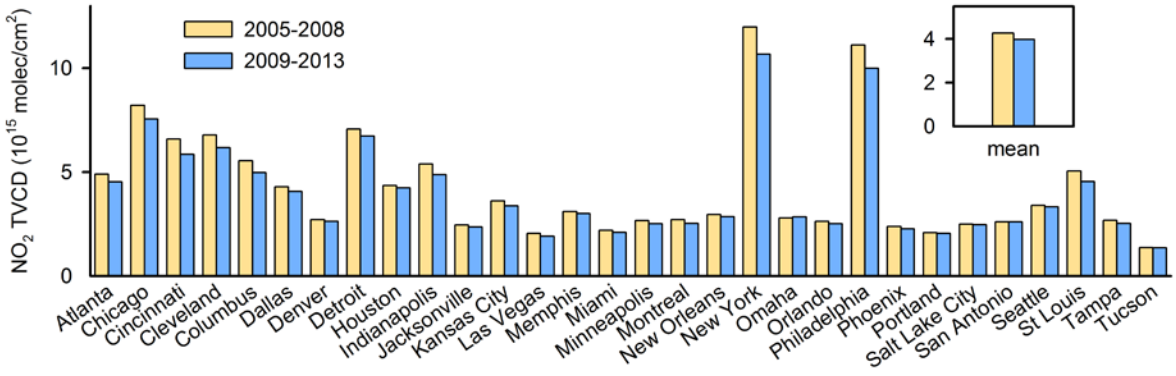

Figure S3. NO_2 TVCDs of investigated cities over the US. The yellow and blue bars denote the mean NO_2 TVCDs in a circle with a radius of 100 km around city centers for the ozone season during 2005–2008 and 2009–2013 respectively. The bars in the inset display the mean NO_2 TVCDs of cities shown.

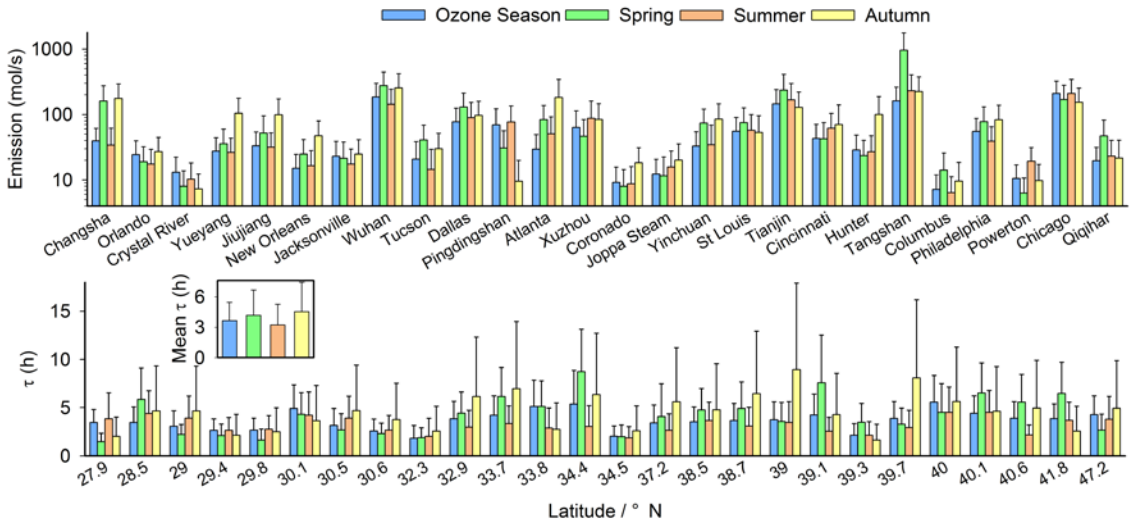

Figure S4. Seasonal mean NO_x emissions and lifetimes. Mean daytime NO_x emissions (top panel) and lifetimes (bottom panel) for the investigated sources (from south to north). The bars in the insets of the bottom panel display the average NO_x lifetimes of sources shown for each season. Error bars show the uncertainties.

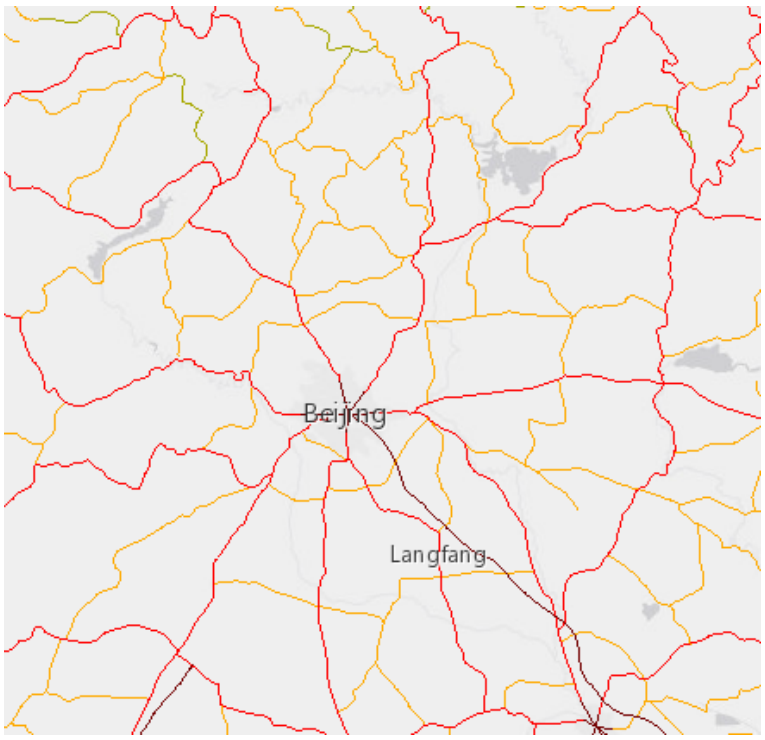

Figure S6. Road-network map of Beijing from the GRIP database. The map is a screen capture of the GRIP website (http://geoservice.pbl.nl/website/flexviewer/index.html?config=cfg/PBL_GRIP.xml).

Reference

Beirle, S., Boersma, K. F., Platt, U., Lawrence, M. G., and Wagner, T.: Megacity emissions and lifetimes of nitrogen oxides probed from space, Science, 333, 1737–1739, 2011.

Beirle, S., Hörmann, C., Penning de Vries, M., Dörner, S., Kern, C., and Wagner, T.: Estimating the volcanic emission rate and atmospheric lifetime of SO_2 from space: a case study for Kīlauea volcano, Hawai'i, Atmos. Chem. Phys., 14, 8309–8322, doi:10.5194/acp-14-8309-2014, 2014.

Boersma, K. F., Eskes, H. J., Veefkind, J. P., Brinksma, E. J., van der A, R. J., Sneep, M., van den Oord, G. H. J., Levelt, P. F., Stammes, P., Gleason, J. F., and Bucsela, E. J.: Near-real time retrieval of tropospheric NO_2 from OMI, Atmos. Chem. Phys., 7, 2103–2118, doi:10.5194/acp-7-2103-2007, 2007.

Boersma, K. F., Eskes, H. J., Dirksen, R. J., van der A, R. J., Veefkind, J. P., Stammes, P., Huijnen, V., Kleipool, Q. L., Sneep, M., Claas, J., Leitão, J., Richter, A., Zhou, Y., and Brunner, D.: An improved tropospheric NO_2 column retrieval algorithm for the Ozone Monitoring Instrument, Atmos. Meas. Tech., 4, 1905–1928, doi:10.5194/amt-4-1905-2011, 2011.

Bucsela, E. J., Krotkov, N. A., Celarier, E. A., Lamsal, L. N., Swartz, W. H., Bhartia, P. K., Boersma, K. F., Veefkind, J. P., Gleason, J. F., and Pickering, K. E.: A new stratospheric and tropospheric NO_2 retrieval algorithm for nadir-viewing satellite instruments: applications to OMI, Atmos. Meas. Tech., 6, 2607–2626, doi:10.5194/amt-6-2607-2013, 2013.

de Foy, B., Lu, Z., Streets, D. G., Lamsal, L. N., and Duncan, B. N.: Estimates of power plant NO_x emissions and lifetimes from OMI NO_2 satellite retrievals, Atmos. Environ., 116, 1–11, 2015.

Dirksen, R. J., Boersma, K. F., Eskes, H. J., Ionov, D. V., Bucsela, E. J., Levelt, P. F., and Kelder, H. M.: Evaluation of stratospheric NO_2 retrieved from the Ozone Monitoring Instrument: Intercomparison, diurnal cycle, and trending, J. Geophys. Res., 116, D08305, doi:10.1029/2010JD014943, 2011.

Fioletov, V. E., McLinden, C. A., Krotkov, N., Moran, M. D., and Yang, K.: Estimation of SO_2 emissions using OMI retrievals, Geophys. Res. Lett., 38, L21811, doi:10.1029/2011gl049402, 2011.

Jöckel, P., Tost, H., Pozzer, A., Kunze, M., Kirner, O., Brenninkmeijer, C. A. M., Brinkop, S., Cai, D. S., Dyroff, C., Eckstein, J., Frank, F., Garny, H., Gottschaldt, K. D., Graf, P., Grewe, V., Kerkweg, A., Kern, B., Matthes, S., Mertens, M., Meul, S., Neumaier, M., Nützel, M., Oberländer-Hayn, S., Ruhnke, R., Runde, T., Sander, R., Scharffe, D., and Zahn, A.: Earth System Chemistry Integrated Modelling (ESCiMo) with the Modular Earth Submodel System (MESSy, version 2.51), Geosci. Model Dev. Discuss., 8, 8635–8750, doi:10.5194/gmdd-8-8635-2015, 2015.

Lamsal, L. N., Martin, R. V., van Donkelaar, A., Celarier, E. A., Bucsela, E. J., Boersma, K. F., Dirksen, R., Luo, C., and Wang, Y.: Indirect validation of tropospheric nitrogen dioxide retrieved from the OMI satellite instrument: Insight into the seasonal variation of nitrogen oxides at northern midlatitudes, J. Geophys. Res., 115, D05302, doi:10.1029/2009JD013351, 2010.

Marchenko, S., Krotkov, N. A., Lamsal, L. N., Celarier, E. A., Swartz, W. H., and Bucsela, E. J.: Revising the slant column density retrieval of nitrogen dioxide observed by the Ozone Monitoring Instrument, J. Geophys. Res., 120, 5670–5692, doi:10.1002/2014jd022913, 2015.

Platt, U., and Stutz, J.: Differential absorption spectroscopy, Springer, Berlin and Heidelberg, Germany, 135–174, 2008.

Russell, A. R., Perring, A. E., Valin, L. C., Bucsela, E. J., Browne, E. C., Wooldridge, P. J., and Cohen, R. C.: A high spatial resolution retrieval of NO_2 column densities from OMI: method and evaluation, Atmos. Chem. Phys., 11, 8543–8554, doi:10.5194/acp-11-8543-2011, 2011.

Valin, L. C., Russell, A. R., and Cohen, R. C.: Variations of OH radical in an urban plume inferred from NO_2 column measurements, Geophys. Res. Lett., 40, 1856–1860, doi:10.1002/grl.50267, 2013.

van Geffen, J. H. G. M., Boersma, K. F., Van Roozendael, M., Hendrick, F., Mahieu, E., De Smedt, I., Sneep, M., and Veefkind, J. P.: Improved spectral fitting of nitrogen dioxide from OMI in the 405–465 nm window, Atmos. Meas. Tech., 8, 1685–1699, doi:10.5194/amt-8-1685-2015, 2015.